SCIENTIFIC REPORTS

OPEN

Improved hole injection for blue phosphorescent organic light-emitting diodes using solution deposited tin oxide nano-particles decorated ITO anodes

Seung Il Lee[1], Geum Jae Yun[1], Jin Wook Kim[3], Gregory Hanta[2], Kunyu Liang[2], Lazar Kojvic[2], Lok Shu Hui[2], Ayse Turak[2] & Woo Young Kim[1,2]

Blue phosphorescent organic light-emitting diodes (PHOLEDs) were fabricated with tin oxide (SnO$_x$) nano-particles (NPs) deposited at the ITO anode to improve their electrical and optical performances. SnO$_x$ NPs helped ITO to increase the work function enhancing hole injection capability. Charge balance of the device was achieved using p- and n-type mixed host materials in emissive layer and the devices' luminance and maximum external quantum efficiency (EQE) increased about nearly 30%. Tuning the work function using solution processed NPs allows rapid optimization of device efficiency.

The evolution of organic light-emitting diodes (OLED) into flat panel display and solid state planar lightning applications has been the result of much development in luminous efficiency, low power consumption and life-time. Among the most significant was the development of doped guest-host matrix systems that utilizing both singlet and triplet excitons for emissions[1–4]. Such phosphorescent OLEDs (PHOLEDs) have significantly higher luminous efficiencies than their fluorescent counterparts, due to the potential for 100% internal quantum efficiency[2]. Further improvements in device performance, such as higher brightness and efficiency, can occur by promoting exciton recombination probability with improved charge injection at interfaces and balance of charge carriers in the emission layer to maximize the formation of photons without losses[5].

In blue PHOLEDs, the blue dopant has a large highest occupied molecular orbital (HOMO) - lowest unoccupied molecular orbital (LUMO) energy band gap, in order to generate blue emission. As a result, the host material should also have a larger energy band gap as well as higher triplet energy level than the blue dopant material allowing Dexter energy transfer and confinement of the triplet excitons. Furthermore, the hole transport material should have high triplet energy level to prevent triplet excitons diffusion into the hole transport layer (HTL) as triplet excitons have longer life-time before they generate phosphorescence and electron mobility is typically faster than hole mobility as voltage increases.

Common materials with large triplet energies used for blue PhOLEDs include, blue dopant material bis[3,5-difluoro-2-(2-pyridyl)phenyl-(2-carboxypyridyl)]-iridium (FIrpic) (T$_1$ = 2.7 eV), host for blue phosphorescent dyes, 1,3-Bis(N-carbazolyl)benzene (mCP) with a large HOMO-LUMO energy gap as well as high triplet energy (=2.9 eV) and HTL materials 1-Bis[4-[N,N-di(4-tolyl)amino]phenyl]-cyclohexane (TAPC) T$_1$ = 2.9 eV and a very deep HOMO level (5.9 eV)[6]. In bottom emission PHOLEDs, generally indium tin oxide (ITO) is used for transparent conducting anodes (ϕ = 4.7 eV), It is generally difficult to inject holes directly into mCP from ITO anodes or a typical HTL such as TAPC due to the large hole injection barrier at the interface. As a result of the large hole injection barriers at the ITO/HTL interface, improvement of carrier injection in blue PHOLEDs is expected to have a more significant effect on the device performance than for green or red PHOLEDs and OLED structures.

A variety of approaches have been used to regulate the work function of ITO including plasma treatment[7], passivation with surface-active species[8], chemical and physical treatments[7,8], halogenation[9], and deposition of

[1]Department of Electronic Display Engineering, Hoseo University, Asan, 31499, South Korea. [2]Department of Engineering Physics, McMaster University, Hamilton, Ontario, L8S 4L7, Canada. [3]Department of Electrical and Electronic Engineering, The University of Hong Kong, Pokfulam Road, Hong Kong, China. Correspondence and requests for materials should be addressed to A.T. (email: turaka@mcmaster.ca) or W.Y.K. (email: wykim@hoseo.edu)

high-work- function metals, insulating materials, and oxides[9–12]. Particularly, inserting metal oxide thin layers such as MoO_3, WO_3, and V_2O_5 between ITO and HTL by thermal evaporation was seen to reduce the energy barrier between ITO and HTL, enhancing hole injection at the interface in OLEDs[13]. As ITO has a very heterogenous surface, the thickness of these buffer layers are critical to optimizing device performance and sub-monolayer films are highly effective in tuning device performance[12,14]. As thermal evaporation can be difficult to control in the sub-monolayer deposition regime for many interlayer materials, a solution based approach can allow more control over the device properties[10,15]. The possibility of tailoring the work function to match the energy level of the active organic layer is of great interest in the fabrication of organic devices to form barrier-free Ohmic contacts.

Tin dioxide (SnO_2) is an n-type metal oxide semiconductor widely used for gas sensors[16,17], ion battery electrodes[18], electrodes for electrochromic devices[19], and interlayers in inverted organic solar cells[20]. Because of its transparency, work function of nearly 4.8 eV at bulk state[21], and tunable electrical conductivity with oxygen vacancy concentration and size[22,23], it is also a potentially interesting interlayer for OLEDs.

Due to their n-type character, SnO_2 has been successfully used as an electron injection layer in inverted OLEDs[24] and organic photovoltaics (OPVs)[20,25–27]. For instance, solution based SnO_2 NPs were deposited as an electron injection layer (EIL) in an inverted OLED structure to eliminate the energy barrier between the metal anode and electron transport layer (ETL)[24]. However, it has not been widely used as a hole injection layer.

Our interest in using it here stems from three major factors. First, it has been shown that electron acceptors can effectively tune the hole injection properties for regular device architectures[14,28,29]. Second, low temperature growth of tin oxides often results in mixed phases, with SnO_2 and SnO coexisting as a result of the metastable nature of SnO[30,31]. Mixed phase alloying has been an effective method of tuning the electronic properties of SnO_x NPs[32]. Finally, the surface of ITO is known to be tin-rich, with SnO_2-like crystalline domains[33–35]. These SnO_x domains are generally thought to be sites of the highest electrical activity[34]. The ITO work function can be controlled by manipulating the proportion of Sn^{4+} ions at the surface with sputtering[36]. By deliberately introducing Sn^{4+} components with submonolayer coverage of SnO_x NPs, we propose an alternative method of controlling the surface electronic structure of ITO for better matching with the deep HOMO of novel HTLs.

In this paper, we introduced SnO_x NPs dispersed on ITO anodes using reverse micelles as a tunable transparent metal oxide material for improving bottom emission blue PHOLEDs electrical and optical properties by improving hole injection at the organic/inorganic interface. By using a solution approach, a uniform distribution of NPs can be deposited on the ITO surface, allowing control and flexibility in the device design.

Increasing the injection of holes using the interfacial NPs layer requires the introduction of a graded mixed-host emitting layer structure to optimize charge balance and improve the EQE by about 30%.

Results

Following the reverse micelle deposition (RMD) process shown schematically in Fig. 1(a) results in a uniform sub-monolayer array of SnO_x NPs (Fig. 1(b)). By limiting the reaction region within the micelles, a mean size of 31.6 ± 2.6 nm, with polydispersity indices[37] of 0.08, were achieved (see Supplemental S1). These particles are large enough to form a sub-monolayer distribution on the ITO surface, while still retaining the electronic properties of bulk tin oxides. As the ITO surface roughness is similar to the mean particle size (RMS = 26.7 nm), the NPs do not increase the roughness. With submonolayer coverage, there appears to be a slight smoothening effect of adding NPs, but the overall surface is substantially similar (see Supplemental S2). To confirm the reproducibility of these results, multiple batches of particles with the same loading ratios were produced on both Si and ITO.

As shown in the EDXS elemental maps of the NPs (Fig. 1(d)) and XPS analysis (Supplemental Fig. S-5), the addition of ethanol to the $SnCl_2$ loaded micelles almost completely consumes the chloride, yielding polycrystalline SnO_x NPs (Fig. 1(c)). Selective area diffraction (inset of Fig. 1(c)) yields powder rings consistent with the 110, 101, 211 and 112 planes of rutile SnO_2[38,39] (see Supplemental S3). XPS characterization (see Supplemental S4) indicates that the tin chloride precursor, solvent and polymeric micelles are completely removed during the multi-step formation, as expected. High resolution core level analysis shows spectra consistent with SnO_2 NPs[40], having a Sn $3d_{5/2}$ core level peak at 437.35 eV. This is offset by 1.1 eV from bulk SnO_2[41,42] due to a size dependent shift, also observed for LiF NPs produced by the reverse micelle method[9]. The calculated Sn:O atomic weights suggests an oxygen deficient sub-stoichiometric compound is formed. As oxygen vacancies are known to intrinsically n-dope SnO_2, a deficient structure is beneficial in maintaining high conductivities in the NPs dispersed surface. This could also be due to the coexistence of the thermodynamically stable rutile phase with metastable SnO, though it is difficult to confirm due to the similarity in the Sn $^{2+}$ and $^{4+}$ 3d core level positions[41,43,44].

Figure 2(a) shows the expected band structure of our blue PHOLED device. The introduction of SnO_x NPs increases the work function of the ITO by 0.27 eV as determined by photoemission yield spectroscopy (see Supplemental S5), similar to previous work with RMD sol-LiF[12]. Though SnO_2 is generally thought of as an n-type semiconductor, and therefore has been recently introduced into inverted type structures as an electron injecting layer[20,24–26], this increase in surface work function with electron accepting organic molecules has been observed previously[14,28,29]. Hong et al. saw a similar increase in ITO work function with a thin layer of C_{60} at the interface between ITO and NPB[29]. It may also be due to the increase in the Sn^{4+} ions on the surface. ITO is known to have a Sn-rich surface[33], with the work function controlled by the relative abundance of Sn^{4+} ions on the surface. Che et al. showed that decreasing the Sn^{4+} fraction with Ar^+ sputtering led to a decrease in the surface work function[36]. The high work function of ITO generally after cleaning was established to be the result of fully oxidized SnO_2 domains at the Sn-rich surface of ITO[36]. As the ITO surface structure is generally inhomogenous, with submonolayer coverage of SnO_x NPs, we are likely deliberately increasing the Sn^{4+} fraction on the surface, leading to an increased work function, relative to the exposed ITO areas. This shift therefore would be due to the intrinsically higher work function of SnO_x as compared to ITO (~0.1–0.2 eV)[21]. The density of dipoles is increased at the surface by isolated SnO_x NPs and their interactions decrease the effect of the surface dipole moment[12,15,45,46].
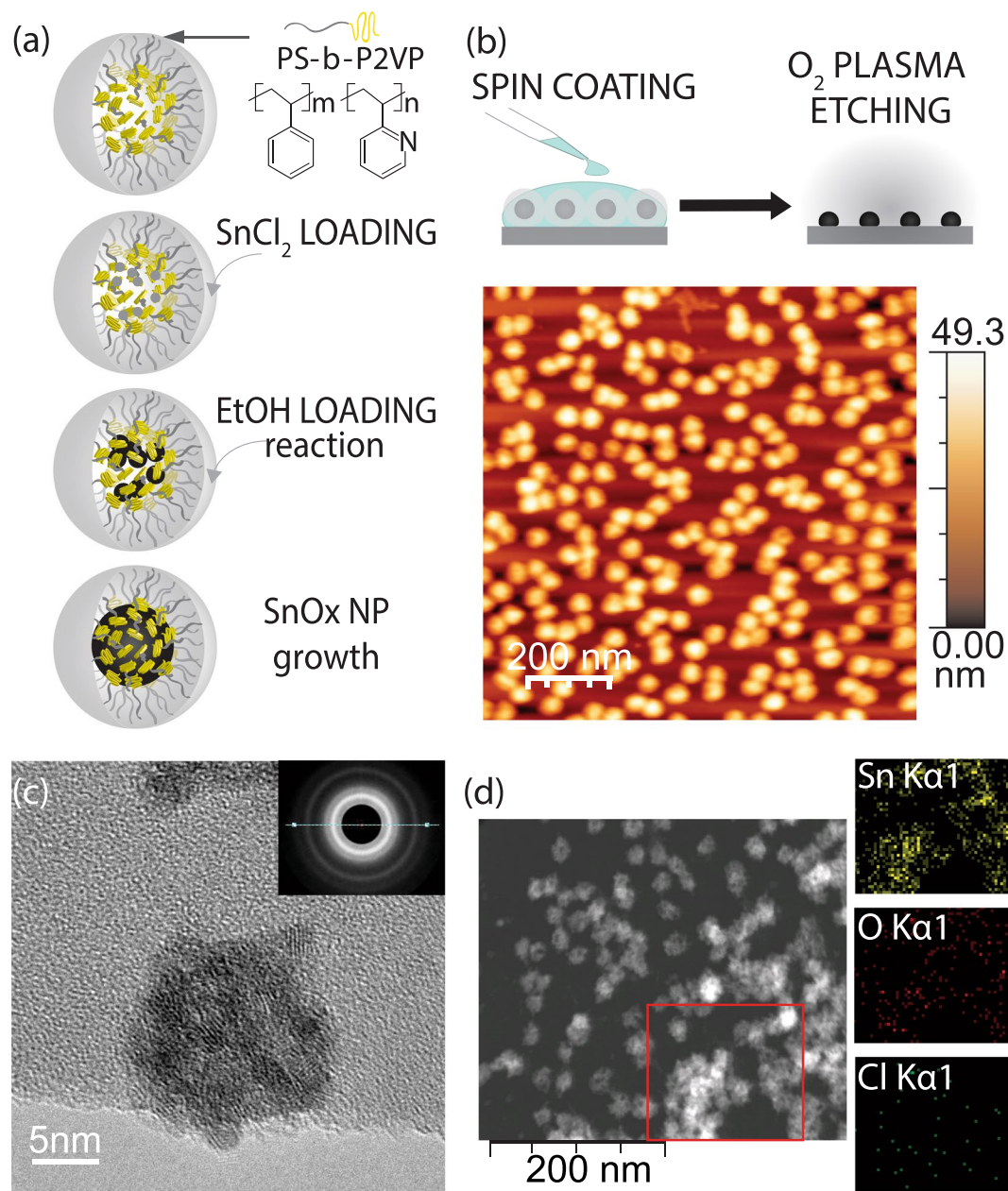
Figure 1. (**a**) Schematic of formation mechanism of SnO$_x$ NPs using a PS-P2VP diblock co-polymer reverse micelle. Sequential loading of the precursors salt results in the formation of polycrystalline NPs from the amalgamation of nucleated nanocrystalline domains. (**b**) Atomic force micrograph of monolayer arrays of NPs formed by spin coating and O$_2$ plasma etching. (**c**) High resolution transmission electron micrograph of polycrystalline SnO$_x$ NPs. Inset shows the selective area electron diffraction pattern. (**d**) Energy dispersive electron spectroscopy elemental maps of NPs deposited on a TEM grid showing the distribution of Sn, O and Cl.

As this moves the anode work function closer to the HOMO energy level of the TAPC as HTL, it lowers the barrier to hole injection at the ITO/HTL interface. This adjustment of the surface work function has been used to improve performance in both OLEDs and OPVs using a variety of dipole modifying approaches including plasma cleaning, chemical modification and presence of interlayers. Both Schottky thermionic emission and Folwer-Nordheim tunneling (see Supplemental Equations S1 and S2) will be improved by the reduction of the barrier, and will improve as a function of voltage.

Another possibility is the simultaneous coexistence of SnO$_2$ with SnO or carbon incorporation into the NPs. Figure 1(d) shows that the NPs tend to be a polycrystalline agglomerate of smaller particles with amorphous regions that could be C, or amorphous Sn oxides. Carbon is known to stabilize NPs and alloying with C has been an effective method of tuning the electronic properties of SnO$_x$ NPs[32]. Given our use of diblock co-polymer micelles for the formation of the NPs, it is likely that some carbon has been incorporated into the SnO$_x$ matrix.
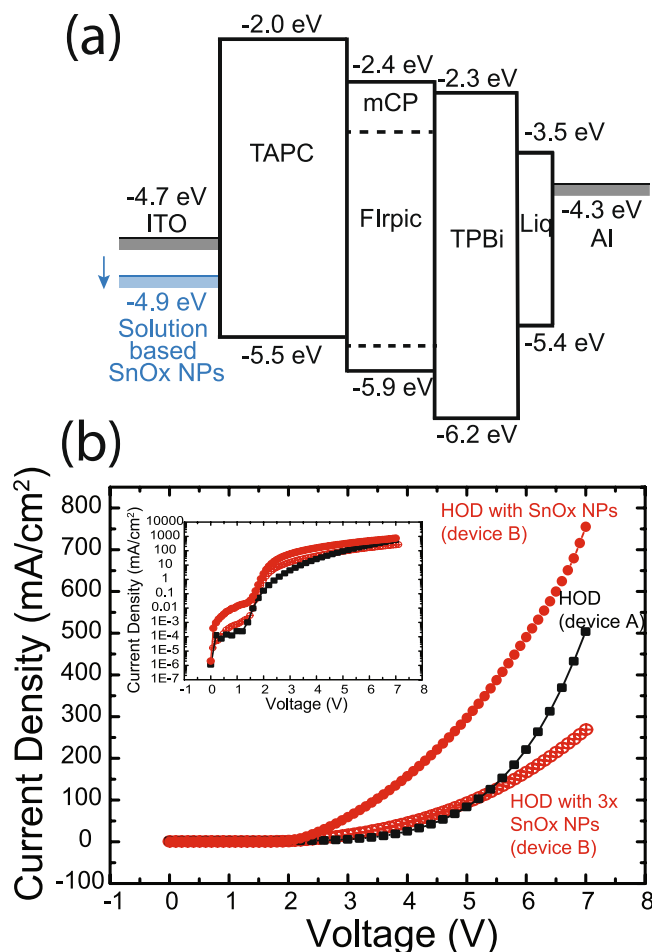
Figure 2. (**a**) Schematic band diagram of PHOLED devices showing the hole injection lowering effect of the SnO$_x$ NPs. (**b**) Current-density voltage (J–V) curves for hole only devices based on TAPC with and without SnO$_x$ NPs (device A and B). Submonolayer NP and complete films (3x) are shown for SnO$_x$ NPs. All devices were exposed to 30 min of O$_2$ plasma etching.

Alternatively, there could be amorphous and/or Sn^{2+} phases incorporated into the NPs. SnO has been used for high mobility p-type thin film transistors[47–49], due to its high hole conductivity through divalent tin vacancies. Though the SAD data is not consistent with stannous tin monoxide, SnO$_2$ and SnO are known to coexist during low temperature deposition as a result of the metastable nature of SnO[30,31]. Due to the similarity of the Sn 3d core level positions for both Sn $^{2+}$ and Sn^{4+} ions[41,43,44], it is difficult to confirm the existence of SnO. The presence of p-type SnO, possibly in the amorphous portions, could improve the injection of charge carriers.

The phenomenon of greater hole injection can be observed in HOD tests based on ITO/TAPC (100 nm)/Al (120 nm). To ensure that the effect is not due to the plasma etching of the ITO surface, the device without NPs was also plasma etched for 30 mins before deposition of TAPC. As shown in the J–V curves of Fig. 2(b), with the addition of SnO$_x$ NPs, higher current density is detected at low voltage and continues to increase as the voltage increases, resulting in a higher slope. Consequently, HODs with SnO$_x$ NPs obtained nearly 450 mA/cm^2 of current density but reached only at 193 mA/cm^2 without SnO$_x$ NPs at 6V, with higher charge carrier effect in the space charge limited current (SCLC) curve, as expected. However, the improvement in injection occurs only when there is a submonolayer coverage of NPs on the ITO surface. As seen in Fig. 2(b), depositing multiple layers of NPs until there is a closed layer (3x spin coating and plasma etching) results in a loss of hole injection.

Recently Mazhari, Rivizi and Mantri[50,51] proposed a new metric, $G = \frac{dlog(J)}{dlog(V)}$, to determine the onset of various current regimes of organic diodes based on the derivative of current density with respect to voltage. As derivative functions are more sensitive to slope changes, such a metric as a function of voltage shows a maximum at the transition voltage between an exponential current based on overcoming the potential barrier at the electrode, and the power law dependent trap-limited and SCLC[51]. It is possible to observe more than one maximum, particularly in systems with traps, suggesting multiple conduction regimes as a function of applied voltage. In a unipolar device, this transition voltage should be proportional to the built-in potential, driven by the difference between the work function of the electrodes[50]. Therefore, changes to the transition voltage can indicate changes to the barrier for charge flow through the device.
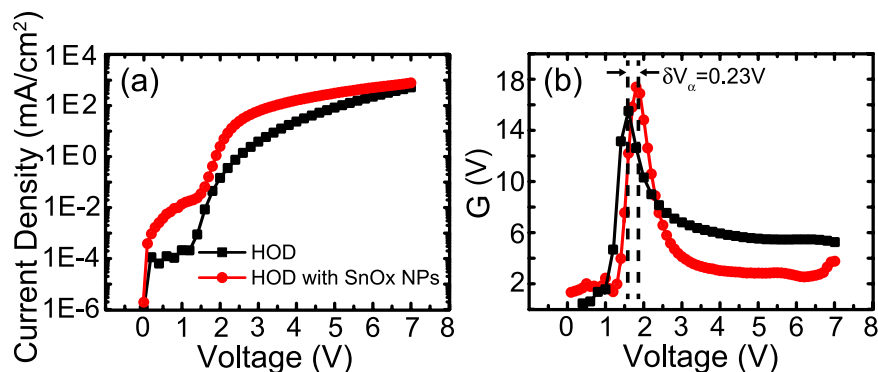
Figure 3. (**a**) Current-density voltage (J–V) curves for hole only devices based on TAPC with and without SnO_x NPs (device A and B). Both devices were exposed to 30 min of O_2 plasma etching. (**b**) G–V characteristics where G represents the derivative function, $G = \frac{dlog(J)}{dlog(V)}$. The peak in G(V) represents the transition voltage between exponential and power-law dependent current-voltage regimes.
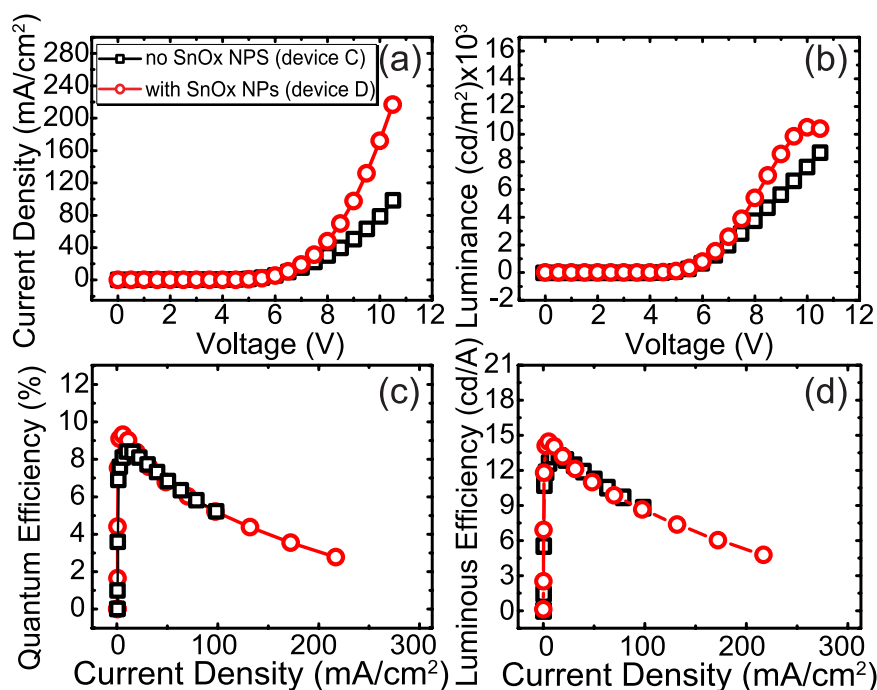
Figure 4. Electric characteristic of blue PHOLEDs with p-host EML, including SnO_x NPs (**a**) current density (J–V) (**b**) luminance (L–V) (**c**) quantum efficiency and (**d**) luminous efficiency as a function of current density.

Figure 3 shows the J–V and G–V curves for the HODs, where an increase in the transition voltage of 0.23 V is observed due to the introduction of NPs. This is consistent with the expected barrier lowering observed with the increase in the ITO surface work function. Additionally, beyond the transition voltage, G(V) is proportional to the power law exponent, m, of the J–V characteristics, and can indicate if the system has entered into a trap-limited ($m > 2$) or space-charge limited conduction regime ($m \approx 2$)[50]. Without SnO_x NPs, the exponent is over 4 (4.3 ± 0.1 from 8 devices), suggesting that the transition voltage indicates the onset of trap-limited current. With SnO_x NPs, the exponent drops to 1.68, indicating that the increased injection of holes allows the device to reach the SCLC regime under lower applied voltage.

When a single submonolayer layer of SnO_x NPs were included in blue PHOLEDs using a p-type host material (mCP) for the emitting layer, devices with a NPs interlayer showed higher luminance and current density as shown in Fig. 4 and Table 1, as was expected from the HOD tests. The luminous and quantum efficiencies were also increased by roughly 10–11% by using the SnO_x NPs as shown in Fig. 4(c,d) compared to the device without NPs (device C). To get adequate statistics, we examined a number of devices and reported the average values, along with the error in Table 1. Devices with SnO_x NPs appear more consistent, with a slightly narrower distribution of efficiency values compared to devices without ITO surface modification. This might arise from the slight smoothening of the ITO surface with NPs or introducing a homogenous distribution of Sn^{4+} containing NPs on

5

Device	EQE(MAX)	EQE(at6V)	LE(MAX)	LE(at6V)	PE(MAX)	PE(at6V)
p-host (device C)	8.9 ± 0.4	8.5 ± 0.6	14.2 ± 0.7	13.5 ± 1.0	7.5 ± 0.5	7.0 ± 0.5
p-host/SnO$_x$ NPs (device D)	9.2 ± 0.2	9.2 ± 0.2	14.5 ± 0.4	14.5 ± 0.4	7.9 ± 0.3	7.6 ± 0.2
mixed host (device E)	8.6 ± 0.8	8.4 ± 0.7	13.9 ± 1.2	13.5 ± 1.0	8.0 ± 0.4	7.1 ± 0.5
mixed host/SnOx NPs (device F)	11.0 ± 0.3	10.5 ± 0.2	17.8 ± 0.5	17.3 ± 0.3	10.4 ± 0.7	9.0 ± 0.2

Table 1. Average device efficiency values for blue PHOLED devices.

the typically inhomogenous ITO surface. Decoration of inhomogenous ITO with LiF NPs has been previously shown to produce more uniform potential surfaces[9]. From our device results, it appears that at lower voltages, the current density is bulk diffusion limited rather than injection limited, with more holes swept into the EML, and the overall yield of excitons is increased. However, considering the increased number of holes in the EML observed in device D, we expected a greater improvement in the luminous and quantum efficiencies. A mismatch in the current density and efficiency suggests a charge imbalance within the device[52–54]. In such devices, improving the injection of charge carriers that are already in excess may improve the absolute current density and luminance due to the greater probability of charge recombination, but lead to minimal increases or even lowered efficiency if the number of excess holes, N''_h, greatly exceeds the number of electron hole pairs ($N'_e = N'_h$). If the hole and injection currents are not equal, the charge balance factor, γ (Eq. 1), may be less than 1, limiting the quantum efficiency.

$$\gamma = \frac{J'_{Cn} - J'_{An}}{J} = \frac{J'_{Cp} - J'_{Ap}}{J} = \frac{N'_h + N'_e}{N''_h + N'_h + N'_e} \qquad (1)$$

Generally, transporting holes is relatively easier than electrons in most organic devices. TAPC as HTL and mCP[55] as the EML host material have hole mobilities of ~1.0×10^{-2} and 3.2×10^{-4} cm^2/Vs respectively, orders of magnitude larger than for the ETL layer, TPBi, which has a typical electron mobility of ~$3.3–8 \times 10^{-6}$ cm^2/Vs[56,57]. In our PHOLED structure, we used mCP as a host material because of the high triplet energy and high quantum yield when used with FIrpic as a blue dopant[6]. Although mCP has only a slightly lower electron mobility than hole mobility ($\mu_e = 2.0 \times 10^{-4}$ cm^2/Vs)[55], the mismatch in the charge carriers leads to a buildup of excitons forming at the mCP/TPBi interface and diffusing into the EML. This suggests that as more holes are injected with the barrier lowering effect of the SnO$_x$ NPs, the number of excess holes in the EML increases, increasing current density while keeping the luminous efficiency almost unchanged.

Therefore, to improve performance, we optimized the charge balance in the device, by incorporating a graded p-/n-type mixed host for part of the emission layer[58,59]. Using mCP:TPBi with a 1:2 ratio at the right side of the EML significantly improved the electron mobility, as has also been observed in white PHOLEDs[54]. TPBi is a well known n-type electron transporting material and has also been used as an n-type host material[59,60]. In such a structure without NPs (device E), due to rapid electron injection into p-/n- mixed host, the current density and luminance is again improved, but the quantum efficiency is almost unchanged, this time due to the increased density of electrons. The increased electron injection led to a decreased efficiency roll-off due to the extension of the recombination zone compared with the standard device with only a p-type host (device C). Additionally, modifying the EML host results in an approximately 0.75 V decrease in the turn-on voltage, but only a slight change in the x,y chromaticity coordinates (see Supplemental Fig. S-6). Having both increased hole injection with a SnO$_x$ NPs, and increased electron mobility with a p-/n-type mixed host achieving higher charge balance, the charge optimized structure results in ~30% increase in the quantum efficiency comparing device E and F (Fig. 5 and Table 1).

This is a much larger increase than that observed for more traditional HIL, such as thin films of MoO$_3$, WO$_3$, and Vd$_2$O$_5$ in blue PHOLEDs. Chiu and Chuang[13] produced blue PHOLEDs with various thin oxide interlayers deposited by sputtering. Though they proposed a similar mechanism of reducing the barrier at the interface by using high work function interlayers, they actually observed no change or a loss in the absolute current density or luminance for every interlayer. Additionally, unlike in our system where we observed ~30% improvement with an optimized device for the EQE, power efficiency and luminance efficiency, they only observed improvements varying from 2–18%, with average increase in the EQE of 3%, PE of 11% and current efficiency of 7%. This may be a result of not optimizing the EML to accommodate increased hole current, or due to the lack of active Sn^{4+} sites on the surface to improve the charge injection.

Conclusions

Originally blue PHOLEDs are known to have low luminous efficiency and high driving voltage due to large barriers to charge injection at interfaces. However, we demonstrated highly efficient blue PHOLEDs by tuning the surface electronic structure of the anode using solution processed SnO$_x$ NPs on the ITO. The current density was significantly increased in both HODs and in blue PHOLEDs due to the increased hole injection from ITO to the TAPC HTL with a submonolayer coverage of SnO$_x$ NPs. Increasing the coverage to achieve a complete layer significantly suppressed hole injection. Charge balance was optimized using a mixed host EML to improve luminance, luminous, quantum and power efficiency. In our study, turn-on voltage was not significantly reduced, suggesting that further optimization is possible with this system. Deliberately introducing Sn^{4+} components with submonolayer coverage of SnO$_x$ NPs is a versatile method of controlling the surface electronic structure of ITO. Reducing the energy barrier to improve hole injection capability through dispersed NPs on the anodes could
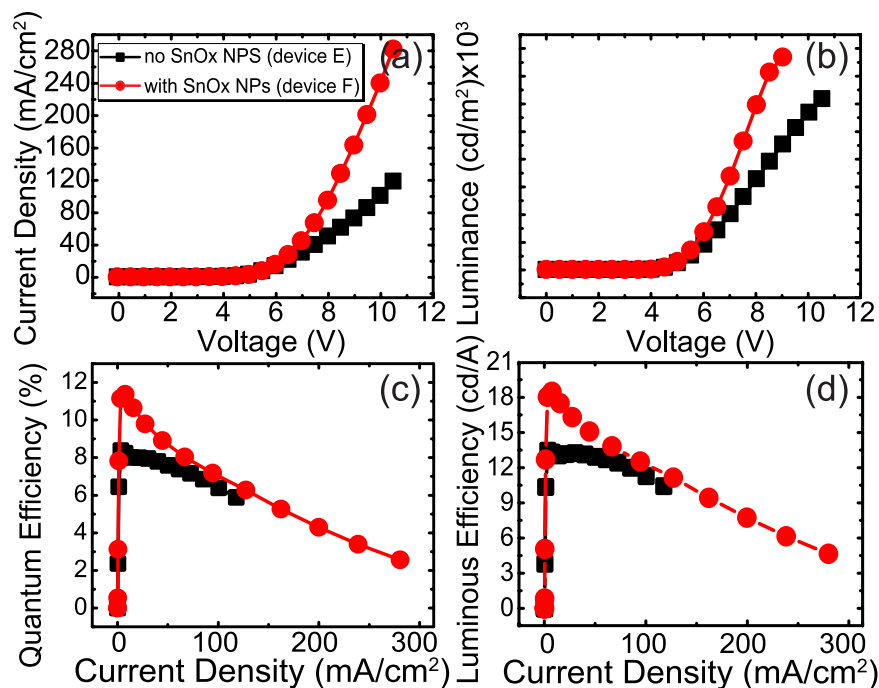
Figure 5. Electric characteristic of blue PHOLEDs, including SnOx NPs, with a p-/n- mixed host EML layer for charge balance optimization (**a**) current density (J–V) (**b**) luminance (L–V) (**c**) quantum efficiency and (**d**) luminous efficiency as a function of current density.

Device No.	Device Structures (Unit : nm)
Device A	ITO/TAPC (100)/Al (120)
Device B	ITO/SnOx NPs/TAPC (100)/Al (120)
Device C	ITO/TAPC (70)/mCP:FIrpic-8% (30)/TPBi (30)/Liq (2)/Al (120)
Device D	ITO/SnOx NPs/TAPC (70)/mCP:FIrpic-8% (30)/TPBi (30)/Liq (2)/Al (120
Device E	ITO/TAPC (70)/mCP:FIrpic-8% (20)/mCP:TPBi (1:2):FIrpic-8% (10)/TPBi (30)/Liq (2)/Al (120)
Device F	ITO/SnOx NPs/TAPC (70)/mCP:FIrpic-8% (20)/mCP:TPBi (1:2):FIrpic-8% (10)/TPBi (30)/Liq (2)/Al (120)

Table 2. Details of device structures.

replace organic buffer layers in thermally activated delayed fluorescent (TADF) OLEDs or deep blue OLEDs requiring even greater HOMO-LUMO energy band gap EML materials.

Method

For SnOx NPs synthesized in solution, polystyrene-block-poly-2-vinylpyridine (PS-b-P2VP) di-block copolymer (polymer source, P1330-S2VP) was dissolved in 5 ml o-xylene and stirred for at least 24 hours. After forming spherical reversed micelles, 10 mg tin-chloride (Alfa Aesar Korea, $SnCl_2$ anhydrous) and 0.3 ml of ethanol was added sequentially in the solution, with constant stirring of at least 48 hours after each loading step. The solution was then centrifuged to remove any precipitates. A monolayer of SnOx-loaded micelles was deposited on various substrates by spin-coating at 2000 rpm, followed by an O_2 plasma etching under 950 mTorr, 29.6 W for 25 min to remove the polymeric micelles and solvent. Transmission electron microscopy/scanning transmission electron microscopy (JEOL 2010F TEM/STEM) operating at 200 kV was carried out to acquire the morphological and structural information of the SnOx NPs. In addition, the NPs are characterized using energy dispersive x-ray spectroscopy (EDXS) on the STEM. Silicon nitride membrane window TEM grids (0.05 × 0.05 mm × 10 nm, Norcada) were utilized to facilitate the spin coating and oxygen plasma process, which allowed the direct TEM/STEM observation of the NPs. We spin-coated SnOx NPs on Si wafers to confirm monolayer formation by atomic force microscopy (AFM) before fabricating blue OLED devices. AFM was done in air in tapping mode with a phase locked loop (PLL) dynamic measurement board (Asylum). The non-contact silicon tips were OTESPA (Asylum) with a resonance frequency of 300 kHz, a force constant of 26 N/m and a tip radius of curvature 7 nm. The AFM images were processed with WSxM (NanoTec). Work function of ITO with SnOx NPs was measured by photoemission yield spectroscopy.

ITO coated glasses were cleaned in an ultrasonic bath sequentially with deionized water, acetone, deionized water and isopropyl alcohol, and dried in a N_2 stream. A monolayer of SnOx NPs was deposited onto the pre-cleaned ITO glass substrates, and cleaned again in a N_2 stream. Hole only devices (HODs) and blue PHOLED

devices were fabricated by thermal evaporation under high vacuum conditions of 5.0×10^{-7} Torr. The complete device structure was composed of TAPC as HTL, mCP as host material, FIrpic as blue dopant material, 2,2′,2″-(1,3,5-Benzinetriyl)-tris(1-phenyl-1-H-benzimidazole) (TPBi) as ETL, Lithium 8-quinolinolate (Liq) as EIL. The cathode electrode, aluminum, was also deposited by thermal evaporation. The devices were then encapsulated in an inert N_2 glovebox using a getter sheet. Specific details of the device structures are outlined in Table 2. The electrical and optical characteristics of blue PHOLED as well as HODs were measured by an I-V-L system.

References

1. Baldo, M. A. *et al.* Highly efficient phosphorescent emission from organic electroluminescent devices. *Nature* **395**, 151–154 (1998).
2. Adachi, C., Baldo, M. A., Thompson, M. E. & Forrest, S. R. Nearly 100% internal phosphorescence efficiency in an organic light-emitting device. *Journal of Applied Physics* **90**, 5048–5051 (2001).
3. Holmes, R. J. *et al.* Blue organic electrophosphorescence using exothermic host–guest energy transfer. *Appl. Phys. Lett.* **82**, 2422–2424 (2003).
4. Tokito, S. *et al.* Confinement of triplet energy on phosphorescent molecules for highly-efficient organic blue-light-emitting devices. *Appl. Phys. Lett.* **83**, 569–571 (2003).
5. Chopra, N., Lee, J. & So, F. Balance in Blue Phosphorescent Organic Light Emitting Diodes. *SID Symp. Dig. Tech. Pap.* **40**, 410–412 (2009).
6. Kawamura, Y. *et al.* 100% phosphorescence quantum efficiency of Ir(III) complexes in organic semiconductor films. *Appl. Phys. Lett.* **86**, 071104 (2005).
7. Milliron, D. J., Hill, I. G., Shen, C., Kahn, A. & Schwartz, J. Surface oxidation activates indium tin oxide for hole injection. *J. Appl. Phys.* **87**, 572–576 (2000).
8. Kim, J. S. *et al.* Indium–tin oxide treatments for single- and double-layer polymeric light-emitting diodes: The relation between the anode physical, chemical, and morphological properties and the device performance. *J. Appl. Phys.* **84**, 6859–6870 (1998).
9. Aytun, T., Turak, A., Baikie, I., Halek, G. & Ow-Yang, C. W. Solution-processed LiF for work function tuning in electrode bilayers. *Nano Lett.* **12**, 39–44 (2012).
10. Zilberberg, K., Meyer, J. & Riedl, T. Solution processed metal-oxides for organic electronic devices. *J. Mater. Chem. C* **1**, 4796 (2013).
11. Tokito, S., Noda, K. & Taga, Y. Metal oxides as a hole-injecting layer for an organic electroluminescent device. *J. Phys. D: Appl. Phys.* **29**, 2750 (1996).
12. Ow-Yang, C. W. *et al.* Work function tuning of tin-doped indium oxide electrodes with solution-processed lithium fluoride. *Thin Solid Films* **559**, 58–63 (2014).
13. Chiu, T.-L. & Chuang, Y.-T. Spectral observations of hole injection with transition metal oxides for an efficient organic light-emitting diode. *J. Phys. D: Appl. Phys.* **48**, 075101 (2015).
14. Koch, N. *et al.* Tuning the hole injection barrier height at organic/metal interfaces with (sub-) monolayers of electron acceptor molecules. *Appl. Phys. Lett.* **87**, 101905 (2005).
15. Turak, A., Aytun, T. & Ow-Yang, C. W. Solution processed LiF anode modification for polymer solar cells. *Appl. Phys. Lett.* **100**, 253303 (2012).
16. Korotcenkov, G. Metal oxides for solid-state gas sensors: What determines our choice? *Materials Science and Engineering: B* **139**, 1–23 (2007).
17. Watson, J. The tin oxide gas sensor and its applications. *Sensors and Actuators* **5**, 29–42 (1984).
18. Idota, Y., Kubota, T., Matsufuji, A., Maekawa, Y. & Miyasaka, T. Tin-Based Amorphous Oxide: A High-Capacity Lithium-Ion-Storage Material. *Science* **276**, 1395–1397 (1997).
19. Olivi, P., Pereira, E. C., Longo, E., Varella, J. A. & Bulhões, L. O. de S. Preparation and Characterization of a Dip-Coated SnO2 Film for Transparent Electrodes for Transmissive Electrochromic Devices. *J. Electrochem. Soc.* **140**, L81–L82 (1993).
20. Trost, S. *et al.* Tin Oxide (SnOx) as Universal "Light-Soaking" Free Electron Extraction Material for Organic Solar Cells. *Adv. Energy Mater.* **5**, 1500277 (2015).
21. Minami, T., Miyata, T. & Yamamoto, T. Work function of transparent conducting multicomponent oxide thin films prepared by magnetron sputtering. *Surface and Coatings Technology* **108**, 583–587 (1998).
22. Batzill, M., Chaka, A. M. & Diebold, U. Surface oxygen chemistry of a gas-sensing material: SnO2(101). *EPL* **65**, 61 (2004).
23. Cabot, A. *et al.* Synthesis of Tin Oxide Nanostructures with Controlled Particle Size Using Mesoporous Frameworks. *Electrochem. Solid-State Lett.* **7**, G93–G97 (2004).
24. Lee, H., Kang, C.-M., Park, M., Kwak, J. & Lee, C. Improved Efficiency of Inverted Organic Light-Emitting Diodes Using Tin Dioxide Nanoparticles as an Electron Injection Layer. *ACS Appl. Mater. Interfaces* **5**, 1977–1981 (2013).
25. Trost, S., Zilberberg, K., Behrendt, A. & Riedl, T. Room-temperature solution processed SnOx as an electron extraction layer for inverted organic solar cells with superior thermal stability. *J. Mater. Chem.* **22**, 16224–16229 (2012).
26. Tran, V.-H., Ambade, R. B., Ambade, S. B., Lee, S.-H. & Lee, I.-H. Low-Temperature Solution-Processed SnO2 Nanoparticles as a Cathode Buffer Layer for Inverted Organic Solar Cells. *ACS Appl. Mater. Interfaces* **9**, 1645–1653 (2017).
27. Barbé, J. *et al.* Amorphous Tin Oxide as a Low-Temperature-Processed Electron-Transport Layer for Organic and Hybrid Perovskite Solar Cells. *ACS Appl. Mater. Interfaces* **9**, 11828–11836 (2017).
28. Zhang, L. *et al.* Origin of Enhanced Hole Injection in Organic Light-Emitting Diodes with an Electron-Acceptor Doping Layer: p-Type Doping or Interfacial Diffusion? *ACS Appl. Mater. Interfaces* **7**, 11965–11971 (2015).
29. Hong, I. H. *et al.* Effective hole injection of organic light-emitting diodes by introducing buckminsterfullerene on the indium tin oxide anode. *Appl. Phys. Lett.* **87**, 63502 (2005).
30. Song, P. & Wen, D. Experimental Investigation of the Oxidation of Tin Nanoparticles. *J. Phys. Chem. C* **113**, 13470–13476 (2009).
31. Chetri, P., Choudhury, B. & Choudhury, A. Room temperature ferromagnetism in SnO2 nanoparticles: an experimental and density functional study. *J. Mater. Chem. C* **2**, 9294–9302 (2014).
32. Bhatnagar, M., Kaushik, V., Kaushal, A., Singh, M. & Mehta, B. R. Structural and photoluminescence properties of tin oxide and tin oxide: C core–shell and alloy nanoparticles synthesised using gas phase technique. *AIP Advances* **6**, 095321 (2016).
33. Frank, G., Köstlin, H. & Rabenau, A. X-ray and optical measurements in the In2O3-SnO2 system. *Phys. Status Solidi A* **52**, 231–238 (1979).
34. Armstrong, N. R., Veneman, P. A., Ratcliff, E., Placencia, D. & Brumbach, M. Oxide contacts in organic photovoltaics: characterization and control of near-surface composition in indium-tin oxide (ITO) electrodes. *Acc. Chem. Res.* **42**, 1748–1757 (2009).
35. Fan, J. C. C. & Goodenough, J. B. X-ray photoemission spectroscopy studies of Sn-doped indium-oxide films. *Journal of Applied Physics* **48**, 3524–3531 (1977).
36. Che, H. & El Bouanani, M. Effects of argon sputtering and UV-ozone radiation on the physico-chemical surface properties of ITO. *Nuclear Instruments and Methods in Physics Research Section B: Beam Interactions with Materials and Atoms* **414**, 170–175 (2018).
37. Yu, H. & Turak, A. Nanoreactors or nanoscale stablizers: routes for solution processed indium tin oxide nanoparticles by reverse micelle deposition. *Can. J. Phys.* **92**, 797–801 (2014).
38. JCPDS-International Centre for Diffraction Data. *Selected powder diffraction data for metals and alloys: data book.* (The Centre, 1978).
39. Tin dioxide (SnO2) crystal structure, lattice parameters, thermal expansion. in *Non-Tetrahedrally Bonded Elements and Binary Compounds I* (eds Madelung, O., Rössler, U. & Schulz, M.) **41C**, 1–2 (Springer-Verlag, 1998).
40. Wang, Y. D., Ma, C. L., Li, H. D. & Zhang, S. Synthesis and characterization of the composite of SnO2 nanoparticles coated on SiO2 microspheres. *Materials Chemistry and Physics* **107**, 248–253 (2008).

41. Themlin, J.-M. *et al.* Characterization of tin oxides by x-ray-photoemission spectroscopy. *Phys. Rev. B* **46**, 2460 (1992).
42. Kövér, L. *et al.* Electronic structure of tin oxides: High-resolution study of XPS and Auger spectra. *Surface and Interface Analysis* **23**, 461–466 (1995).
43. Stranick, M. A. & Moskwa, A. SnO by XPS. *Surface Science Spectra* **2**, 45–49 (1993).
44. Mannie, G. J. A. *et al.* X-ray photoelectron spectroscopy study on the chemistry involved in tin oxide film growth during chemical vapor deposition processes. *Journal of Vacuum Science & Technology A: Vacuum, Surfaces, and Films* **31**, 01A105 (2012).
45. Kim, S. Y. *et al.* Rhodium-oxide-coated indium tin oxide for enhancement of hole injection in organic light emitting diodes. *Appl. Phys. Lett.* **87**, 072105 (2005).
46. Kim, S. Y., Lee, J.-L., Kim, K.-B. & Tak, Y.-H. Enhancement of hole injection using iridium-oxide-coated indium tin oxide anodes in organic light-emitting diodes. *Appl. Phys. Lett.* **86**, 133504 (2005).
47. Um, J. & Kim, S. E. Homo-Junction pn Diode Using p-Type SnO and n-Type SnO2 Thin Films. *ECS Solid State Lett.* **3**, P94–P98 (2014).
48. Caraveo-Frescas, J. A. *et al.* Record Mobility in Transparent p-Type Tin Monoxide Films and Devices by Phase Engineering. *ACS Nano* **7**, 5160–5167 (2013).
49. Ogo, Y. *et al.* p-channel thin-film transistor using p-type oxide semiconductor, SnO. *Appl. Phys. Lett.* **93**, 032113 (2008).
50. Mantri, P., Rizvi, S. M. H. & Mazhari, B. Estimation of built-in voltage from steady-state current–voltage characteristics of organic diodes. *Org. Electron.* **14**, 2034–2038 (2013).
51. Rizvi, S. M. H., Mantri, P. & Mazhari, B. Traps signature in steady state current-voltage characteristics of organic diode. *J. Appl. Phys.* **115**, 244502 (2014).
52. Yu, S.-Y., Huang, D.-C., Chen, Y.-L., Wu, K.-Y. & Tao, Y.-T. Approaching Charge Balance in Organic Light-Emitting Diodes by Tuning Charge Injection Barriers with Mixed Monolayers. *Langmuir* **28**, 424–430 (2012).
53. Kim, S. Y. *et al.* Correlation Between Charge Injection and Charge Balance in Organic Light Emitting Diodes Using LiF and IrO x Interlayers. *J. Electrochem. Soc.* **156**, J57–J61 (2009).
54. Chin, B. D., Suh, M. C., Lee, S. T., Chung, H. K. & Lee, C. H. Improved blue light-emitting polymeric device by the tuning of drift mobility and charge balance. *Appl. Phys. Lett.* **84**, 1777 (2004).
55. Jou, J.-H. *et al.* High-efficiency blue organic light-emitting diodes using a 3,5-di(9H-carbazol-9-yl)tetraphenylsilane host via a solution-process. *J. Mater. Chem.* **20**, 8411–8416 (2010).
56. Wong, T. C., Kovac, J., Lee, C. S., Hung, L. S. & Lee, S. T. Transient electroluminescence measurements on electron-mobility of N-arylbenzimidazoles. *Chemical Physics Letters* **334**, 61–64 (2001).
57. Lee, H., Ahn, H. & Lee, C. Device characteristics of blue phosphorescent organic light-emitting diodes depending on the electron transport materials. *J. Inf. Disp.* **12**, 219–222 (2011).
58. Kim, J. W. *et al.* Study of p/n Type Co-Host System in Single Emissive White Phosphorescent Organic Light-Emitting Devices Using Glass and Flexible Substrate. *Sci. Adv. Mater.* **8**, 1634–1640 (2016).
59. Lee, J. Y. Mixed-host-emitting layer for high-efficiency organic light-emitting diodes. *J. Inf. Disp.* **15**, 139–144 (2014).
60. Wang, J. *et al.* High efficiency green phosphorescent organic light-emitting diodes with a low roll-off at high brightness. *Organic Electronics* **14**, 2854–2858 (2013).

Acknowledgements

Author Contributions

Seung Il Lee performed main experiments, prepared Figures 2, 4 and 5 and wrote the main manuscript text. Ayse Turak prepared Figures 1, 3, S-4 and S-5 and contributed to revising the main manuscript with Woo Young Kim. Geum Jae Yun supported device experiments, Gregory Hanta measured AFM images and prepared Figures S-1 and S-2, Kunyu Liang performed the TEM, EELS, and SAD measurements and prepared Tables S-1 and S-3. Jin Wook Kim, Lazar Kojvic, Lok Shu Hui participated in this research and reviewed the manuscript.

Additional Information

Supplementary information accompanies this paper at https://doi.org/10.1038/s41598-019-39451-4.

Competing Interests: The authors declare no competing interests.

Publisher's note: Springer Nature remains neutral with regard to jurisdictional claims in published maps and institutional affiliations.